36. For large values of $\eta\Omega_d\tau$, we expect $\alpha(\tau)$ to saturate because of nonlinear correction factors that limit the amplitude of the coherent state and introduce amplitude squeezing [see (31) and W. Vogel and R. L. de Matos Filho, *Phys. Rev. A* **52**, 4214 (1995)]. For the experimental Lamb-Dicke parameter of ~0.2, these corrections are not significant for $\alpha \leq 5$.
37. J. F. Poyatos, J. I. Cirac, P. Zoller, in preparation.
38. D. T. Smithey, M. Beck, M. G. Raymer, A. Faridani, *Phys. Rev. Lett.* **70**, 1244 (1993); S. Wallentowitz and W. Vogel, *ibid.* **75**, 2932 (1995); J. I. Cirac and P. Zoller, in preparation.
39. We acknowledge key assistance from W. M. Itano, D. Leibfried, J. C. Bergquist, and J. Erickson and useful discussions with J. I. Cirac, P. Zoller, and D. Walls. We thank M. Young, S. Mechels, and D. Lee for critical comments on the manuscript. This work is supported by the U.S. Office of Naval Research and the U.S. Army Research Office.

2 January 1996; accepted 6 March 1996

The Whole Structure of the 13-Subunit Oxidized Cytochrome c Oxidase at 2.8 Å

Tomitake Tsukihara, Hiroshi Aoyama, Eiki Yamashita, Takashi Tomizaki, Hiroshi Yamaguchi, Kyoko Shinzawa-Itoh, Ryosuke Nakashima, Rieko Yaono, Shinya Yoshikawa*

The crystal structure of bovine heart cytochrome c oxidase at 2.8 Å resolution with an *R* value of 19.9 percent reveals 13 subunits, each different from the other, five phosphatidyl ethanolamines, three phosphatidyl glycerols and two cholates, two hemes A, and three copper, one magnesium, and one zinc. Of 3606 amino acid residues in the dimer, 3560 have been converged to a reasonable structure by refinement. A hydrogen-bonded system, including a propionate of a heme A (heme a), part of peptide backbone, and an imidazole ligand of Cu_A, could provide an electron transfer pathway between Cu_A and heme a. Two possible proton pathways for pumping, each spanning from the matrix to the cytosolic surfaces, were identified, including hydrogen bonds, internal cavities likely to contain water molecules, and structures that could form hydrogen bonds with small possible conformational change of amino acid side chains. Possible channels for chemical protons to produce H_2O, for removing the produced water, and for O_2, respectively, were identified.

Cytochrome c oxidase is the terminal oxidase of cell respiration, a process that reduces molecular oxygen to water with the electrons from cytochrome c, coupled to pumping protons from the matrix side of the mitochondrial membrane toward the cytosolic side (intermembrane space) (*1*). This enzyme contains two iron sites and two copper sites (Fe_a, Fe_{a3}, Cu_A, and Cu_B) in addition to zinc and magnesium sites (*1*). The protein moiety is composed of 13 different polypeptide subunits (*2*), three encoded by mitochondrial genes and ten by nuclear genes (*3*). Because of its physiological importance and the intriguing reaction catalyzed, this enzyme has been studied as one of the most important subjects in bioenergetics since its discovery (*4*). However, the difficulty in purification and crystallization of the large multicomponent membrane protein (*5*) has prevented determination of the crystal structure at an atomic resolution that could lead to the elucidation of the reaction mechanism.

Crystals of cytochrome c oxidase isolated from beef heart muscle have been obtained and the three-dimensional structure was solved at 2.8 Å resolution (*6*). These structures of metal sites confirmed earlier proposals that were based on mutagenesis and spectrophotometric data on, for example, ligand binding residues for hemes a and a_3 and Cu_B, the binuclear structure of Cu_A, and the relative locations of Fe_a, Fe_{a3}, and Cu_B. Unexpectedly, no direct bridging ligand from amino acids was observed between Fe_{a3} and Cu_B. We now describe the structure of the protein moiety and nonprotein constituents other than metals, which

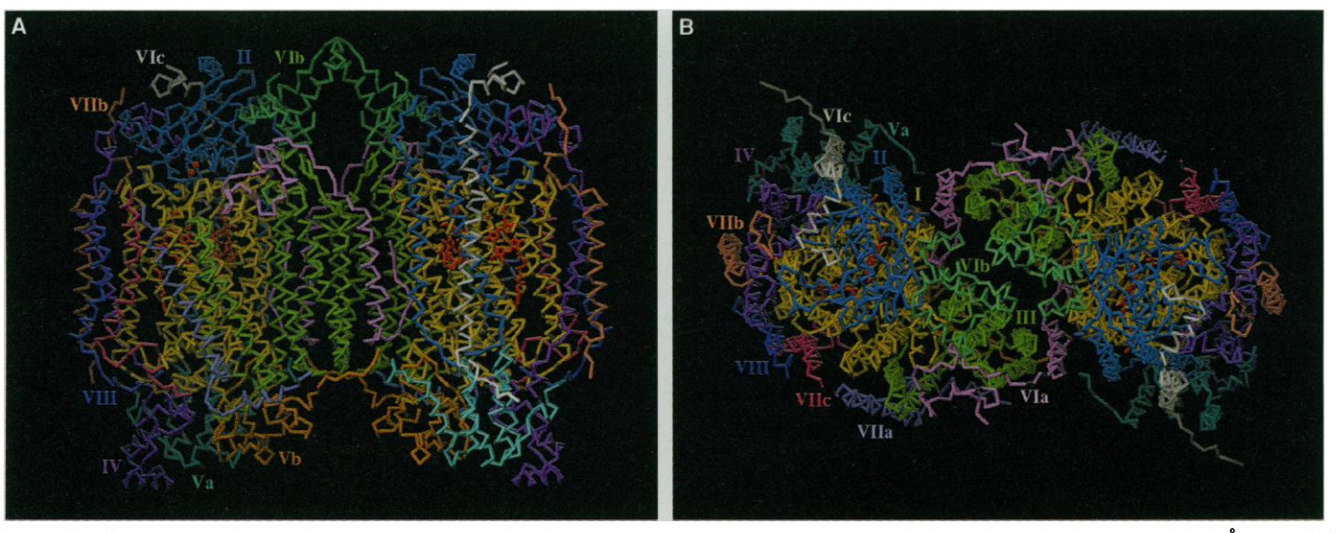

Fig. 1. The Cα-backbone trace of dimer of bovine heart cytochrome c oxidase. Crystallization, intensity data collection, phase determination and a procedure of density modification (*20*) have been described (*6*). Positional refinement followed by temperature factor refinement with program X-PLOR (*27*) reduced the *R* factor to 0.199 and the R_{free} to 0.252 at 2.8 Å resolution. The root mean square (rms) deviations from standard values of bond length and angles for the refined structure were 0.012 Å and 1.73°, respectively. Each monomer consists of 13 different subunits. (**A**) A view to the transmembrane surface and (**B**) a view from the cytosolic side. Both figures contain hemes a and a_3 and two Cu atoms of the Cu_A site (red). Each subunit has a different color with the subunit name in the color of the subunit (Brookhaven Protein Data Bank number, 1OCC).

show possible proton, water, and O_2 channels as well as a possible structure for the facile electron transfer between Cu_A and heme a. The structure of the related bacterial cytochrome c oxidase has been described, and its three major common subunits show many structural similarities to the bovine enzyme (7).

Overall protein structure. The asymmetric unit of the unit cell, shown with C_α backbones (Fig. 1, A and B), is composed of two monomers, each containing 13 different polypeptide subunits in the protein moiety. Of 3606 amino acid residues in an asymmetric unit composed of a dimer, structural models of 3560 residues as well as those of metal centers were successfully built into the electron density map. In addition to these components, eight lipids and two cholic acids were found in the electron density map. The molecular mass of the monomer calculated for the protein moiety is 204,005 kD and that for the other constituents (except for the cholic acid) identified so far in the electron density map is 6998. Polar amino acid residues occur chiefly at the top and bottom of the molecule, an indication that the middle portion, which is composed of 28 α helices per monomer, is the transmembrane part of the molecule. A view from the cytosolic side (Fig. 1B) shows that the two monomers are facing each other around a quasi-twofold symmetric axis. The surface of each monomer facing the other is concave, forming a large opening between them.

All the peptides in the transmembrane region defined as above, except for the 10 amino acid residues in the NH_2-terminal of subunit VIa and two segments of the interhelix regions from Gly^{121} to Tyr^{129} and from Val^{287} to Met^{292} of subunit I are in an α-helical conformation. Comparison of our data on the transmembrane helices with those predicted for subunits I, II, and III from the amino acid sequences (3, 8) (Fig. 2) indicates that the number of transmembrane α helices were correctly predicted. However, most of the real helix regions are longer than predicted, and an interhelix region between Val^{287}, and Met^{297} in subunit I, including two Cu_B ligands, His^{290}, and His^{291}, was predicted to be part of a transmembrane α helix region. The presence of transmembrane α helix has been successfully predicted for the nuclear-coded subunits from the analysis of the location of the NH_2- and COOH-terminals, that is, seven of ten subunits have transmembrane regions (3) (Fig. 2).

Subunits encoded by mitochondrial genes. Subunit I, located mainly in the transmembrane domain, consists of 12 transmembrane helices, without any large extramembrane part (Fig. 3A). This subunit is cylindrical and is oriented perpendicularly to the membrane surface. Three semicircular arrangements of transmembrane helices, each composed of four helices, form a "whirlpool" with a quasi-threefold axis of symmetry (Fig. 4, viewed from the top). Two of the three semicircles hold hemes a and a_3, respectively, which are perpendicular to the membrane plane. The twisted hydroxyl farnesylethyl group of heme a_3 intersects the semicircle between helices VIII and IX. These structures are fully consistent with those of bacterial enzyme (7). The helices of subunit I are not completely perpendicular to the membrane surface plane, but one end of each helix is placed on the top left and the other end on the bottom right (angles of 20° to 35° against the vertical line from the membrane plane) when the cytosolic surface of subunit I is "up". The extramembrane portion in the

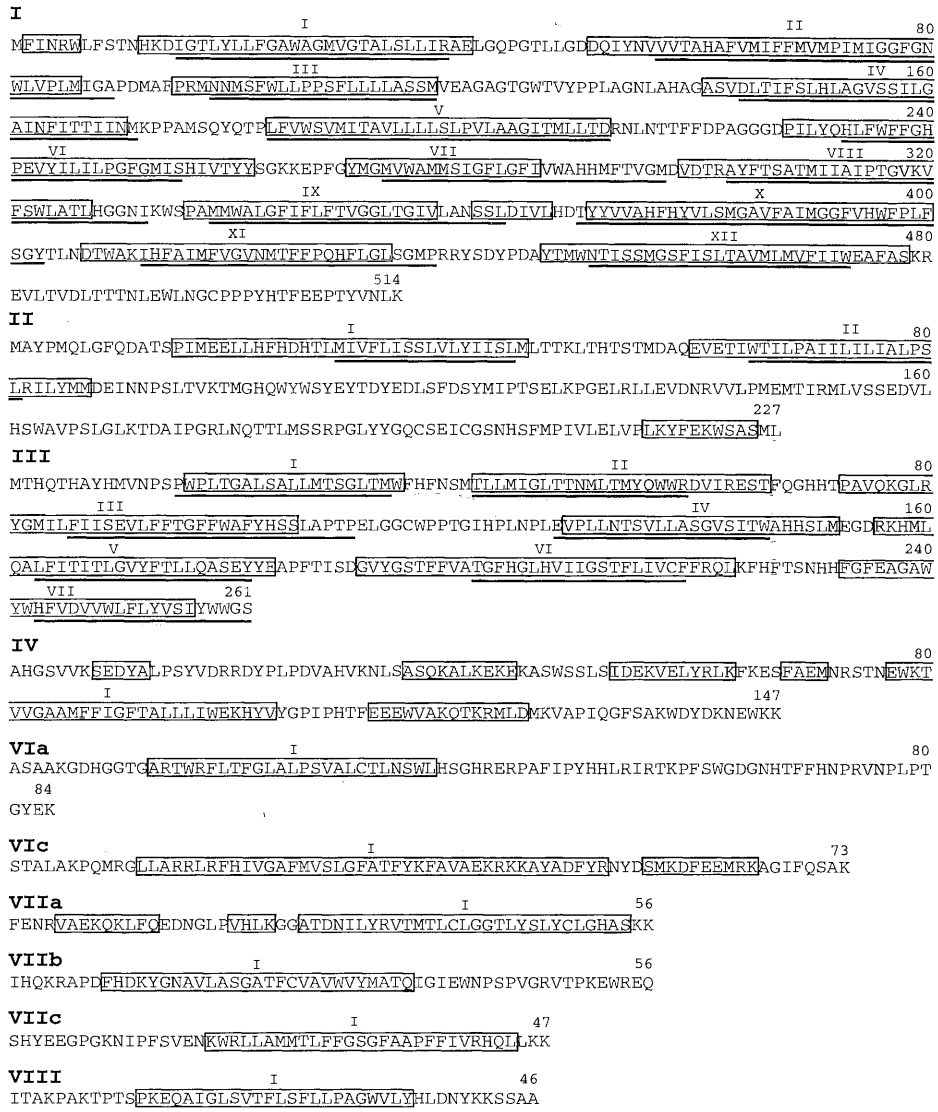

Fig. 2. Helix regions of subunits containing transmembrane moieties. Rectangles denote α-helical regions as determined from the crystal structure; underscoring denotes the α-helical regions predicted from the amino acid sequences. Bold and plain Roman numerals denote subunit name and number of transmembrane helix. Rectangles without a Roman numeral are α helices found in the extramembrane region. No prediction for transmembrane helix region has yet been reported for the nuclear coded subunits. The number of amino acids missing in the crystal structure are as follows; three residues from the NH_2-terminal of subunit IV, ten residues from the NH_2-terminal of subunit VIb, five residues and two residues from the NH_2- and COOH-terminals of subunit VIIb, respectively, and three residues from the COOH-terminal of subunit VIII. Abbreviations for the amino acid residues are: A, Ala; C, Cys; D, Asp; E, Glu; F, Phe; G, Gly; H, His; I, Ile; K, Lys; L, Leu; M, Met; N, Asn; P, Pro; Q, Gln; R, Arg; S, Ser; T, Thr; V, Val; W, Trp; and Y, Tyr.

T. Tsukihara, H. Aoyama, E. Yamashita, T. Tomizaki, H. Yamaguchi are at the Institute for Protein Research, Osaka University, 3-2 Yamada-oka, Suita 565, Japan.
K. Shinzawa-Itoh, R. Nakashima, R. Yaono, S. Yoshikawa are at the Department of Life Science, Himeji Institute of Technology, Kamigohri Akoh, Hyogo 678-12, Japan.

*To whom correspondence should be addressed.

NH_2-terminal region contains a two-turn α helix. The starting and ending points of the 12 helices are essentially at the membrane surface to provide a flat top and bottom surface to the subunit I cylinder. The NH_2- and COOH-terminals of subunit I are on the matrix side. An extramembrane helix between the transmembrane helices IX and X is at the membrane surface, as in the case of bacterial enzyme (7). However, a segment between helices III and IV is in a nonhelical loop, in contrast to the reported α-helical conformation of this region of the bacterial enzyme (7).

Subunits II and III associate with the transmembrane region of subunit I without any direct contact with each other (Figs. 3A and 4). The two transmembrane helices I and II of subunit II are near helices IX and VIII of subunit I, respectively, with antiparallel interactions (Fig. 4 and Table 1). The large extramembrane domain of subunit II is above the cytosolic surface of subunit I and has a 10-strand β barrel structure that holds the Cu_A site 7 Å from the nearest surface atom. The location of the Cu_A indicates the cytosolic side of the enzyme molecule. Both NH_2- and COOH-terminals of subunit II are located on the cytosolic side.

Contact between subunit I and subunit III is made by helices III and IV of subunit I with helix I of subunit III, and helices IV and V of subunit I with helix III of subunit III (Fig. 4 and Table 1). Not all helices are parallel to each other. Helix I of subunit III is at an angle of 20° to helices III and IV of subunit I. Similarly, helix III of subunit III is at an angle of 50° to helices IV and V of subunit I, and also with helix III of subunit III. Subunit III contains seven transmembrane helices with no extensive extramembrane domain (Fig. 3A). The NH_2-terminal is on the matrix side. A big V-shaped cleft is formed between a bundle of helices I and II and the other bundle including helix III and the other helices in a four-helix bundle structure (9) (Fig. 4). One side of the cleft is formed by helices IV and V of subunit I (Fig. 4) and the extramembrane domain of subunit VIa overlays it (Fig. 3B). The bottom side of the cleft, much narrower than the top side, is sealed with an extramembrane α helix of subunit VIIa in the NH_2-terminal region (Fig. 3B). However, the other side of the transmembrane surface is exposed to the external medium (Fig. 4).

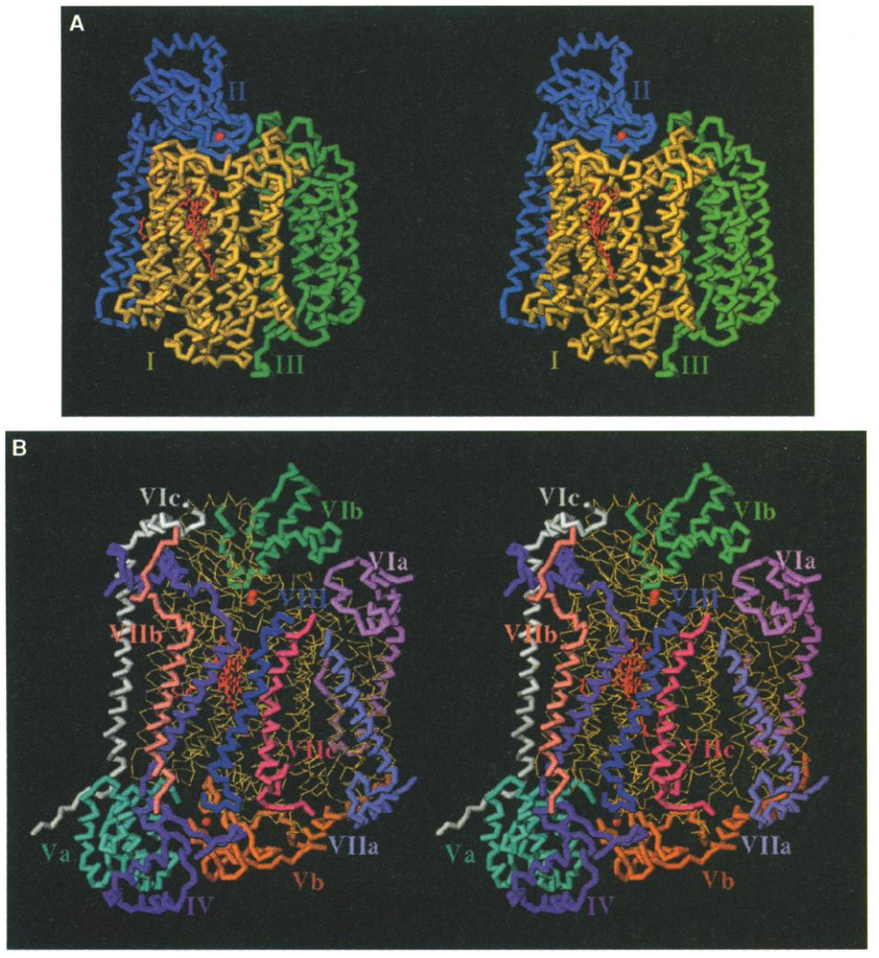

Fig. 3. Stereoscopic drawings of C_α-backbone trace for the 13 different subunits in separate figures. (**A**) Subunits I (yellow), II (blue), and III (green); (**B**) subunits IV (purple), subunits Va (blue), Vb (dark yellow), VIa (pale reddish violet), VIb (blue green), VIc (gray), VIIa (lavender), VIIb (beige), VIIc (pink), and VIII (indigo). A red ball in subunit Vb denotes the zinc atom. Each subunit has the same color as in Figs. 1 and 3. Red models and balls in subunits I and II, respectively, denote hemes and Cu atoms in Cu_A. Subunits I, II, and III are shown by yellow thin stick models in (B).

Nuclear coded subunits, each with a transmembrane helix. Subunit IV looks like a dumbbell with a transmembrane helix in the middle with two extramembrane domains on both ends (Fig. 3B). The cytosolic domain contains two α helices with four turns and only one turn, respectively, with the matrix domain having two α helices, each with three turns. The transmembrane helix contacts diagonally to helices XI and XII of subunit I (Figs. 3B and 4) with an angle of 50°. The transmembrane helix of the subunit IV associates with subunits VIIb and VIII as well as subunit I. The transmembrane helix of subunit IV is sandwiched between helix XII of subunit I and the subunit VIIb helix. Subunit VIIb has an extended structure on the cytosolic side but no extra domain on the matrix side (Fig. 3B). Subunit VIII with an NH_2-terminal short extended structure on the matrix side is adjacent to and in parallel with the transmembrane helix of subunit IV, with close diagonal contacts to helices I and XII of subunit I in the upper and lower transmembrane regions, respectively (Figs. 3B and 4). A part of the NH_2-terminal segment of subunit VIII, from Thr^2 to Lys^4, forms an antiparallel β structure with the COOH-terminal segment of subunit I, from Glu^{481} to Thr^{484} on the matrix side. Adjacent to subunit VIII on the surface of subunit I, subunit VIIc, with a NH_2-terminal small extramembrane moiety in a irregular conformation (Fig. 3B), is placed also with close diagonal packings to helices I and XII of subunit I (Fig. 4). Subunits VIIb, IV, VIII, and VIIc are side by side in that order from left to right (when viewed from the side) with the cytosolic side up and subunit III on the right. To the right of subunit VIIc is subunit VIIa, with an extramembrane region on the matrix side on the surface of subunit III with cross-interactions to its helices I and II (Figs. 3B and 4 and Table 1). The transmembrane helix of this subunit is against subunit III with the COOH-terminal on the cytosolic side near the COOH-terminals of subunit VIIc (Figs. 3B and 4). The three-turn α helix in the NH_2-terminal of subunit VIIa is in plane of the membrane surface on the matrix side, giving a rectangular turn at the membrane surface (Fig. 3B). Subunit VIc is also a dumbbell

type subunit with a transmembrane helix with contact to helix I of subunit II, an extended peptide segment on the matrix side and a four-turn α helix on the cytosolic side parallel to the membrane surface as in the case of the extramembrane α helix of subunit VIIa on the matrix side (Figs. 3B and 4). The transmembrane helix of subunit VIa interacts with helix IV of subunit III on the opposite side of the attachment point of subunit III to subunit I and making contact with the other monomer (Figs. 3B and 4). Ten residues of the NH_2-terminal are in an extended conformation in the transmembrane region in contact with helices V and VII of subunit I of the other monomer (Fig. 4). These contacts seem likely to stabilize the dimeric structure. The electron density distribution for the ten NH_2-terminal residues of subunit VIa is unexplainably less clear than that for the other part of the protein moiety.

As stated above, most of the transmembrane helices are not vertical to the membrane plane and usually are not parallel to each other. Any one of a pair of the nearest-neighbor helices in our crystal structure crosses with the other in any one of three types of stable helix-helix interactions, namely, crossings at one of three angles, approximately, 0°, 20°, or 50° (Table 1) (*10*). These stable packings contribute to the stability of the enzyme molecule, which could be critical, particularly for crystals.

Extramembrane subunits. All three extramembrane subunits are encoded by nuclear genes. Subunit Va, which is on the matrix side below subunit I, contains five α helices, each with four to five turns, forming a right-handed superhelix (Fig. 3B) (*11*). Subunit Va is held without any direct contact to subunit I by the matrix domain of subunit IV and the extramembrane segment of subunit VIc. The shortest distance between two atoms of subunits I and Va is 6.5 Å, indicating that bulk water enters freely into the interspace between them.

Subunit Vb is below subunits I and III, adjacent to subunit Va and toward the extramembrane domain of subunit IV, but without direct contact to subunits IV and Va (Fig. 3B). The subunit attaches tightly to the bottom surfaces of subunits I and III. The COOH-terminal domain of subunit Vb forms a β-barrel structure, involving an extended segment of subunit I, in which a tetrahedral zinc site with four cysteine ligands is located. The NH_2-terminal region of this subunit is in an extended conformation interacting with subunit III. A four-turn α helix segment links the two domains. The subunit folds in an abnormally extended conformation, which is stable only in the subunit assembly. This subunit has a zinc site (*6*) with four cysteines and a zinc finger motif (*12*) in the amino acid sequence between Cys^{60} and Cys^{85}. However, the conformation that we determined does not suggest any physiological role as a zinc finger.

Table 1. Geometries of interaction between two adjacent transmembrane α helices.

Inclination degree	Orientation	Adjacent helices*
~0	Antiparallel	II(**I**)-III(**I**), VI(**I**)-VII(**I**), X(**I**)-XI(**I**), IX(**I**)-I(**II**)
~20	Parallel	I(**I**)-III(**I**), II(**I**)-IV(**I**), III(**I**)-I(**III**), I(**III**)-I(**VIIa**), I(**IV**)-I(**VIIb**), I(**VIIc**)-I(**VIII**)
~20	Antiparallel	I(**I**)-II(**I**), I(**I**)-XII(**I**), III(**I**)-IV(**I**), IV(**I**)-V(**I**), V(**I**)-VI(**I**), VII(**I**)-VIII(**I**), VIII(**I**)-IX(**I**), IX(**I**)-X(**I**), XI(**I**)-XII(**I**), VIII(**I**)-II(**II**), IV(**I**)-I(**III**), I(**II**)-I(**VIc**), I(**III**)-II(**III**), II(**III**)-I(**VIIa**), III(**III**)-IV(**III**), III(**III**)-VII(**III**), IV(**III**)-V(**III**), V(**III**)-VII(**III**), V(**III**)-VI(**III**), VI(**III**)-VII(**III**), IV(**III**)-I(**VIa**),
~50	Parallel	II(**I**)-VI(**I**), II(**I**)-X(**I**), VI(**I**)-X(**I**), I(**I**)-I(**VIIc**), I(**I**)-I(**VIII**), V(**I**)-III(**III**), XI(**I**)-I(**V**)
~50	Antiparallel	II(**I**)-V(**I**), IV(**I**)-III(**III**), XII(**I**)-I(**IV**), XII(**I**)-I(**VIII**)

*Each helix is denoted by a helix number followed by a subunit number in boldface and parenthesis.

Subunit VIb, the only subunit without transmembrane helix on the cytosolic side, associates with subunits II and III (Fig. 3B). Two disulfide bridges are present between Cys^{29} and Cys^{64} and between Cys^{39} and Cys^{53}. The segment between Cys^{39} and Cys^{53} is involved in an intermonomer contact with the corresponding segment on the other monomer around the twofold symmetry axis (Fig. 1B). This structure as well as ten residues of NH_2-terminal of subunit VIa in contact with the other monomer as described above seems to stabilize the dimeric state. The structure suggests that this enzyme functions in the dimeric state under physiological conditions in that both the bridging peptides are coded by nuclear genes. Thus, the dimer state may not be attained in the bacterial enzyme, which lacks these subunits (*7*).

The above assembled structure of this enzyme has a concave surface created by subunits II, VIa, and VIb on top of subunit I, which could form an interaction site for a cytochrome c molecule (about 25 Å in diameter). The following acidic amino acid residues in this region could interact with the basic protein, cytochrome c, to stabilize an enzyme-substrate complex; Asp^{50} and Asp^{221} of subunit I; Glu^{109}, Asp^{119}, Glu^{127}, Asp^{139}, Glu^{157}, and Asp^{158} of subunit II, Glu^{111} of subunit III; and Asp^{74} and Glu^{78} of subunit VIb. There are no contributions of acidic amino acid from subunit VIa. There are positively charged amino acids in the area including His^{51} of subunit VIa, Arg^{75} of subunit VIb and His^{102} of subunit II. Among the above amino acids encoded by mitochondrial genes, Glu^{109} and Asp^{139} of subunit II are well conserved even in bacterial enzymes (*3*), suggesting some indispensable role in binding of cytochrome c.

Nuclear coded subunits associate with the surface of the three core subunits, leaving many areas without any covering, especially on the cytosolic side. All the NH_2-terminal ends of the transmembrane helices of the nuclear coded subunits are placed on the matrix side and the COOH-terminal ends on the cytosolic side. The locations are consistent with those predicted by crosslinking analysis (*3*), except for subunit VIa, whose NH_2-terminal was assigned to be located on the cytosolic side (*13*). This structural feature suggests that these subunits are inserted into the mitochondrial membrane led by the NH_2-terminals.

Metal sites. Metal site structures deter-

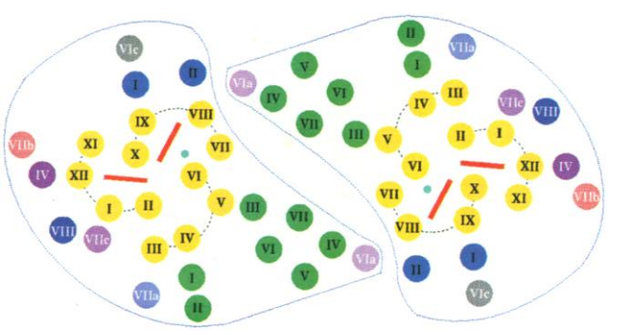

Fig. 4. A schematic representation for location of transmembrane helices as a cross-section at the membrane surface on the cytosolic side. Red bars and a small light blue ball denote heme planes and Cu_B, respectively. Black Roman numerals in yellow, indigo, and green circles denote the helix number of subunits I, II, and III, respectively. White letters in the other circles indicate nuclear coded subunits. Molecular surface of each monomer is shown in a dotted line. Broken lines denote semicircles observed in the helix arrangement of subunit I.

mined without refinement of protein structure (6) have scarcely been modified after the refinement of the protein moiety, which confirms both the reliability of the previous determination and the quality of the electron density distribution described.

Cu_A-Fe_a and Cu_A-Fe_{a3} distances are 20.6 and 23.2 Å, respectively (6), when measured from the central point of the two copper atoms of the Cu_A site to the iron atoms. The structure does not suggest why there is preferential electron transfer from Cu_A to Fe_a without apparent direct electron transfer to Fe_{a3}, as seen experimentally. However, if it is assumed that through-bond versus through-space electron transfer is facilitated (*14*), various networks that could serve as electron transfer paths or control electron transfer can be identified between the Cu_A site and hemes a and a_3. The shortest network and perhaps the most effective, as an electron transfer path between Cu_A and heme a, is a hydrogen bond system including His^{204} of subunit II, a ligand to Cu_A, a peptide bond between Arg^{438} and Arg^{439} of subunit I, and a propionate of heme a (Fig. 5). Similar hydrogen bonds have been found in the bacterial enzyme (*7*). The double-bond character of peptide unit may contribute to the efficiency of the electron conductivity of the network. However, the following two networks could serve as pathways for through-bond electron transfer between Cu_A and heme a_3; a network branched from the shortest network at the peptide linkage between Arg^{439} and Arg^{438} of subunit I, with the latter residue being salt-bridged to a propionate of heme a_3 and another network including Mg site bridged to Cu_A by Glu^{198} of subunit II on one side and to a propionate of heme a_3 by His^{368} of subunit I on the other (Fig. 5). The experimental data so far obtained (*15*) suggest that the two last-mentioned networks are much less effective kinetically than the first and shortest one.

The following aromatic amino acid residues are densely distributed near these redox active sites (Fig. 6) and may control electron transfer through the hydrogen-bond systems or they may enhance the electron transfer through space between the redox sites (*16*). Three tyrosines—Tyr^{440} of subunit I near the His^{204} of subunit II liganded to Cu_A, Tyr^{54}, and Tyr^{371} of subunit I, both near the propionate involved in the shortest hydrogen-bond system between Cu_A and heme a as described above—form a triangle, the plane of which is essentially parallel to the shortest hydrogen-bond system and perpendicular to the plane of heme a. Other tyrosines, Tyr^{443} and Tyr^{447} of subunit I are placed above the tyrosine triangle. The tyrosine system and the Mg site are on opposite sides of the shortest hydrogen-bond system. The three residues of subunit I, Tyr^{371}, Tyr^{443}, and Tyr^{447} are highly conserved. Tyr^{440} of subunit I is replaced in some species with a hydrophobic amino acid like isoleucine or phenylalanine. Conversely, Tyr^{54} of subunit I is replaced with amino acids that could form a hydrogen bond.

This description of the structure around the redox active sites suggests that the preferential electron transfer between Cu_A and heme a is mainly facilitated by the shortest hydrogen-bond system as defined above [and also noted in the bacterial enzyme (*7*)]. However, because of the time scale of the rate of the internal electron transfer reactions between Cu_A and heme a—$t_{1/2}$ of approximately 0.1 msec (*15*)—the much slower reduction of heme a_3 does not seem to be explainable by the absence of any direct electron transfer to heme a_3. It is possible that electrons go from Cu_A to heme a by way of heme a_3 or Cu_B (or both) without any indication of reduction at these intermediate redox sites. Hence these structures contribute to the tightly and delicately interrelated redox system, as has been suggested by the redox behavior of the enzyme under static conditions (*17, 18*).

A major structural difference between the redox active metal sites of beef heart and bacterial enzymes is the ligation of Cu_B (*6, 7*). When the bacterial enzyme is in the azide-bound fully oxidized state, one of the imidazole ligands to Cu_B is missing (*7*). In contrast, the crystal structure of beef heart enzyme without any external ligand shows three imidazoles as the ligands to Cu_B (*6*). The structural difference is probably due to the difference in the ligation, namely, the presence or absence of azide, and not to a difference in the subunit structure. Binding of the ligand may weaken the ligation of His^{290} to Cu_B. In the fully oxidized state of bovine heart enzyme, His^{290} is in a position where it can form a hydrogen bond to the Thr^{309}, which is consistent with the structure assumed (but not detected) by Iwata *et al.* (*7*). For elucidation of the mechanism of the proton pump and possible involvement of imidazole (*19*), it is critical to determine the conformation of the imidazole in other redox and ligand binding states.

Phospholipids. Eight phospholipids, five phosphatidyl ethanolamines (PE) and three phosphatidyl glycerols (PG), have been clearly demonstrated in the multiple isomorphous replacement electron density distribution refined by the density modification method (*20*). The eight phosphorus atoms are located at the membrane surface, either on the cytosolic or matrix sides, and the hydrocarbon tails are directed toward the inside of the transmembrane region as would be expected if these phospholipids are in the lipid bilayer (Fig. 7). One PE and one PG are placed on the cytosolic side and the other six, on the matrix side. Two PEs and one PG are located in the large cleft of subunit III. Thus, the cleft seems to serve as a lipid pool. Three PEs and two PGs surround the transmembrane surface of subunit I on the opposite side from the subunit III contact and one PE on subunit VIa (Fig. 7).

These phospholipids are bound to the protein by salt bridges or hydrogen bonds (or

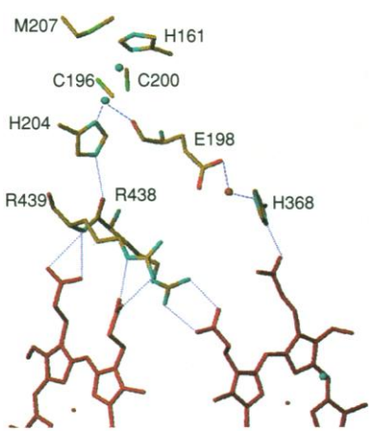

Fig. 5. Hydrogen-bond network between Cu_A, and hemes a and a_3. Amino acid residues, Arg^{439}, Arg^{438}, and His^{368} belong to subunit I; the remaining residues belong to subunit II. Red atomic models with and without a small blue ball (Cu_B) are hemes a_3 and a, respectively. The two copper atoms shown by the two blue balls on the upper side form the Cu_A site with the six amino acids surrounding. A small, dark yellow ball denotes a magnesium atom. The blue, red, and green portions of amino acids denote nitrogen, oxygen, and sulfur atoms, respectively. Dotted lines and broken lines denote hydrogen bond and coordination bond, respectively. Only the bonds forming the network are shown.

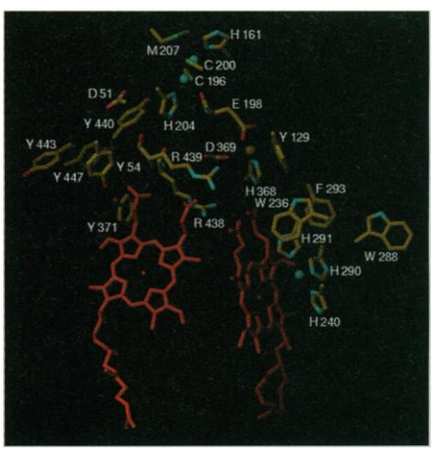

Fig. 6. Arrangement of aromatic amino acids near the redox active metal centers. A pair of blue balls form the Cu_A center. Red structures on the bottom are hemes a and a_3. The blue, red, and green portions of amino acids denote nitrogen, oxygen, and sulfur atoms, respectively.

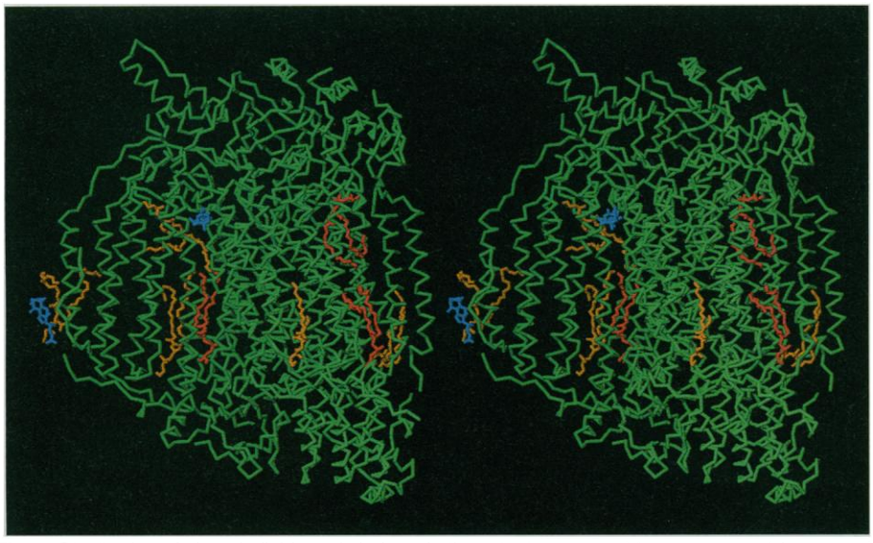

Fig. 7. Distribution of phospholipids and cholates in the cytochrome c oxidase monomer (stereoscopic drawing). Yellow, red, and blue structures are the atomic models of phosphatidyl ethanolamines, phosphatidyl glycerols, and cholic acids, respectively. Each model was deduced from the electron density map obtained.

both) between the polar head groups (phosphate, ethanolamine, and glycerol) and amino acid side chains, main chain imides, or carbonyl groups (Table 2), and also by the hydrophobic interaction between the hydrocarbon tails and the hydrophobic amino acid residues in the transmembrane region. The chain length of the hydrocarbon tails of the phospholipid is assignable in most cases (Table 2). The electron density distribution of unsaturated bonds in the tail remains to be determined.

A phospholipid in the enzyme (PG1) on the bottom of the lipid pool of subunit III shows typically the quality of electron density of the phospholipids detected (Fig. 8). One of the long hydrocarbon tails is in an essentially fully extended conformation in close contact to that of the adjacent phospholipid (PE1). The hydrophilic head group of the phospholipid interacts with subunits I and III, forming a salt bridge between the phosphate group and Arg^{96} of subunit I as well as hydrogen bonds between a hydroxyl of the glycerol group and side chains of His^{71} and Glu^{64} of subunit III (Table 2). Other phospholipids are also clearly observable.

We have found only the above lipids.

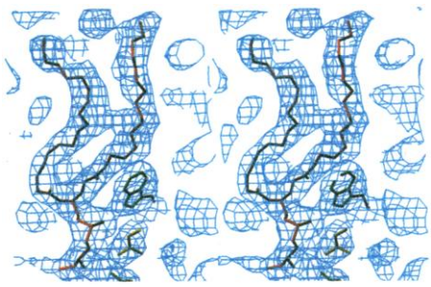

Fig. 8. Fitting of the atomic model of a phosphatidyl glycerol (PG1) to the electron density map (stereoscopic drawing). Red, green, and yellow structures are PG1, Trp^{57} of subunit III, and Arg^{96} of subunit I.

However, cardiolipin has long been known as one of the phospholipids that cannot be removed without loss of the enzyme activity moieties in the enzyme (*21*). Although we have not found cardiolipin, some electron density remains to be examined in the intermonomer space, which is large enough for placing two cardiolipins. Recently, myrystic acid covalently bound to Lys^{324} of subunit I of the *Neurospora crossa* cytochrome c oxidase has been described (*22*). However, we have not found any specific electron density distribution or any space corresponding to such fatty acid around the corresponding residue, Lys^{319}, of beef heart enzyme.

Possible nucleotide-binding sites. Specific electron density cages, in line with the cytosolic and the matrix locations of phospholipids in the enzyme molecule, indicate specific bindings of two cholic acid molecules (Figs. 7 and 9A). The carboxyl group of the one on the cytosolic side has hydro-

Table 2. Structures and locations of phospholipids in the crystal structure.

Phospholipids	Hydrocarbon tails	Subunits (helices)	Amino acids (subunits) interacting with		Level
			Phosphate	Amine (glycerol)	
PE1	C_{18}, C_{20}	**III**(II, III, VI, VII)	R221(**III**),* H231(**III**), S65(**III**), F233*N*(**III**), G234*N*(**III**)	H226*C*(**III**)	L
PE2	C_{18}, C_{20}	**III**(IV, V, VI), **VIa**	I188*N*(**III**), F70*N*(**VIa**), T68(**VIa**)	Y181*C*(**III**), Y182*C*(**III**), F70*C*(**VIa**)	U
PE3	C_{12}, C_6	**I**(VIII), **II**(I, II), **VIc**	D57*N*(**II**), H52(**II**)		L
PE4	C_{10}, C_{20}	**I**(VIII, XI, XII), **IV**, **VIIb**, **VIII**	T408(**I**), H3(**VIIb**)	T408(**I**), E74(**IV**)	L
PE5	C_{18}, C_{20}	**III**(V), **VIa**	R17(**VIa**) OH_{12} of cholate		L
PG1	C_{16}, C_{18}	**I**(III, IV, V), **III**(I, II, III, VI, VII)	R96(**I**),*	[H71(**III**)], [E64(**III**)]	L
PG2	C_{16}, C_{18}	**I**(IX, XI), **II**(I), **VIc**	R43(**VIc**),* G8*N*(**II**)	[K42(**VIc**)]	U
PG3	C_{16}, C_{18}	**I**(IX, XI), **II**(I), **IV**	K49(**II**)*	[K49(**II**)], [N69(**IV**)], [R70*C*(**IV**)]	L

*Salt-bridged. *N, C*; hydrogen bondings via main chain imide or carbonyl, respectively. U, L; placed on the cytosolic or matrix sides, respectively.

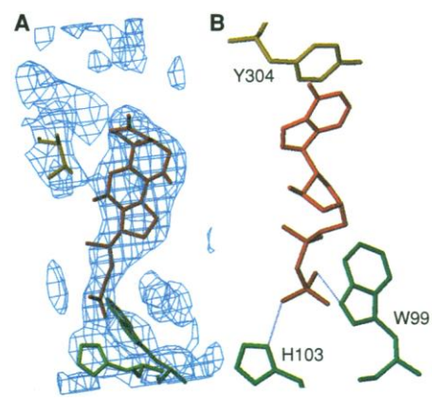

Fig. 9. Electron density map of the possible nucleotide-binding site. (**A**) Fitting of atomic model of cholate (in red) to the electron density map of the cytosolic level binding site. The yellow atomic model denotes Thr^{301} of subunit I and the green models, Trp^{99} and His^{103} of subunit III. (**B**) Fitting of ADP (in red) to the crystal structures of the cholate binding site on the cytosolic level. Tyr^{304} of subunit I in yellow, Trp^{99} and His^{103} of subunit III in green are given. Dotted lines and solid lines in (B) denote hydrogen bonds and salt bridges, respectively.

gen bonds to an imidazole of His[103] of subunit III as well as to an indole of Trp[99] of the same subunit (Fig. 9A). The sterol group of the cholate is located horizontally in the membrane surface plane on the cytosolic side. An OH group at position 12 of the sterol group is also hydrogen-bonded to Thr[301] of subunit I. Thus, the cholate bridges helix III of subunit III and helix VIII of subunit I. The second cholate forms a salt bridge between a carboxyl group of the acid and Arg[14] of subunit VIa. The OH group at position 12 forms a hydrogen bond to the oxygen atom of the phosphoester of PE5. The sterol group is vertical, with the acid terminal on the bottom, in line with the phospholipids on the matrix side (Fig. 7).

The size and shape of ADP resembles that of cholate. The amino acid side chains surrounding the sterol moiety of the bound cholates and those near the carboxyl group are arranged so that ADP or other purine nucleotide with two inorganic phosphates can fit these sites. In fact, an atomic model of ADP fits quite favorably in either the cholate binding sites (Fig. 9B). For the cytosolic cholate site, His[103] and Trp[99] of subunit III form hydrogen bonds with a phosphate group. The phenyl ring of Tyr[304] of subunit I stabilizes the ADP binding by a

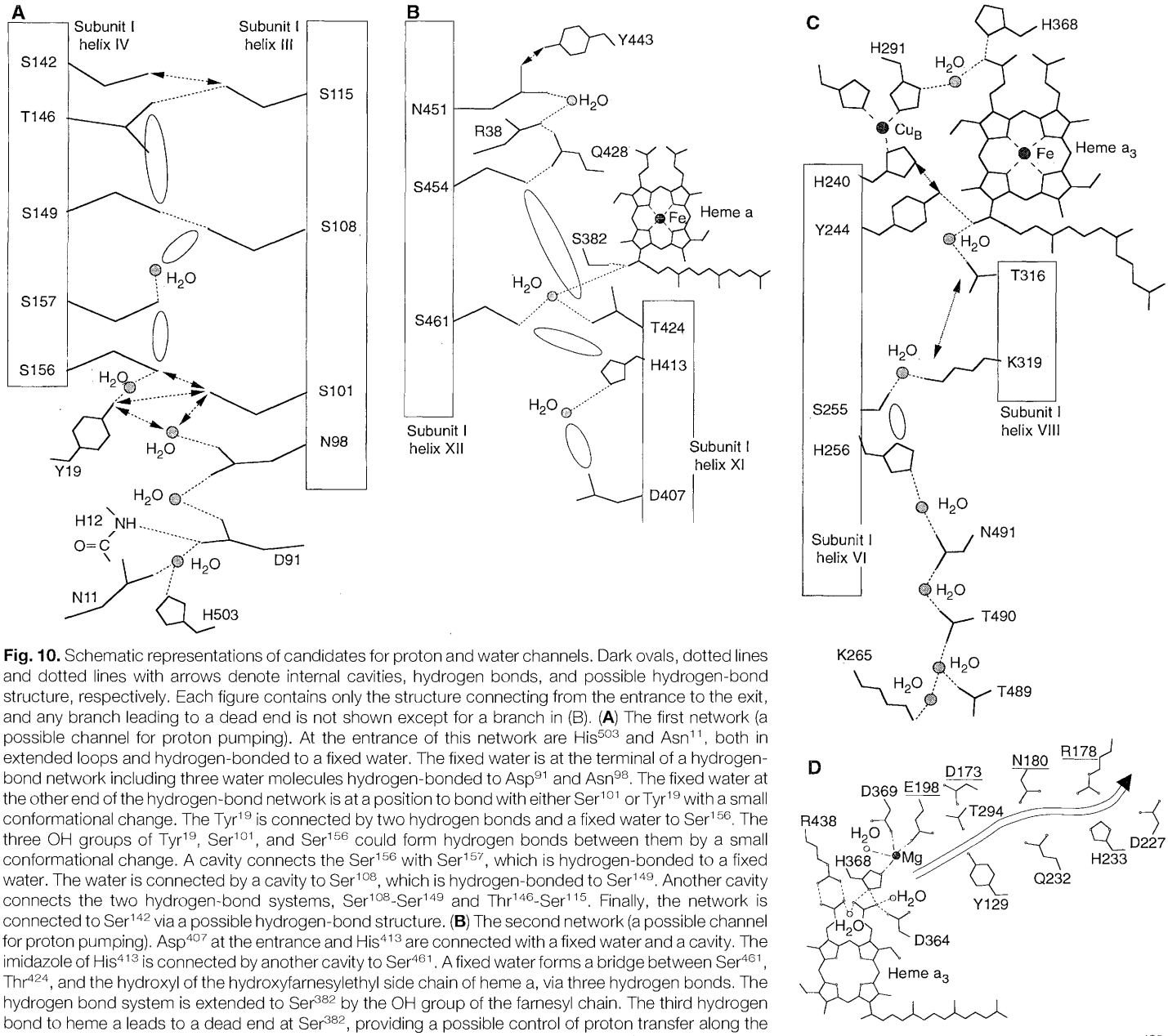

Fig. 10. Schematic representations of candidates for proton and water channels. Dark ovals, dotted lines and dotted lines with arrows denote internal cavities, hydrogen bonds, and possible hydrogen-bond structure, respectively. Each figure contains only the structure connecting from the entrance to the exit, and any branch leading to a dead end is not shown except for a branch in (B). (**A**) The first network (a possible channel for proton pumping). At the entrance of this network are His[503] and Asn[11], both in extended loops and hydrogen-bonded to a fixed water. The fixed water is at the terminal of a hydrogen-bond network including three water molecules hydrogen-bonded to Asp[91] and Asn[98]. The fixed water at the other end of the hydrogen-bond network is at a position to bond with either Ser[101] or Tyr[19] with a small conformational change. The Tyr[19] is connected by two hydrogen bonds and a fixed water to Ser[156]. The three OH groups of Tyr[19], Ser[101], and Ser[156] could form hydrogen bonds between them by a small conformational change. A cavity connects the Ser[156] with Ser[157], which is hydrogen-bonded to a fixed water. The water is connected by a cavity to Ser[108], which is hydrogen-bonded to Ser[149]. Another cavity connects the two hydrogen-bond systems, Ser[108]-Ser[149] and Thr[146]-Ser[115]. Finally, the network is connected to Ser[142] via a possible hydrogen-bond structure. (**B**) The second network (a possible channel for proton pumping). Asp[407] at the entrance and His[413] are connected with a fixed water and a cavity. The imidazole of His[413] is connected by another cavity to Ser[461]. A fixed water forms a bridge between Ser[461], Thr[424], and the hydroxyl of the hydroxyfarnesylethyl side chain of heme a, via three hydrogen bonds. The hydrogen bond system is extended to Ser[382] by the OH group of the farnesyl chain. The third hydrogen bond to heme a leads to a dead end at Ser[382], providing a possible control of proton transfer along the main stream by redox change in heme a. The Thr[424] is connected by a cavity to Ser[454], which is a terminal of another hydrogen bond network including Gln[428], Arg[489], a fixed water, and Asn[451]. The Asn[451] and Tyr[443] are connected by a possible hydrogen-bond structure. (**C**) The third network (a possible channel for protons for releasing water). At the entrance, Lys[265] and Thr[490] are connected via two fixed waters. One of the waters closer to Thr[490] is hydrogen-bonded also to Thr[489], perhaps stabilizing the arrangement of the two water molecules. The hydrogen-bond network is extended up to His[256] via Asn[491] and two water molecules. The His[256] is connected to Lys[319] via a cavity, Ser[255] and a fixed water molecule hydrogen-bonded between Ser[255] and Lys[319]. The lysine is connected by a possible hydrogen-bond structure to Thr[316]. A fixed water forms two hydrogen bonds to Thr[316] and the OH of the hydroxyfarnesylethyl group of heme a_3, which is hydrogen-bonded to Tyr[244]. The Tyr[244] is connected by a possible hydrogen bond structure to His[240], one of the ligands of Cu_B. (**D**) A possible water channel, in which underlined residue names and numbers denote the residues of subunit II. Small circles in the amino acid models are polar atoms. The arrow denotes a possible water channel from the O_2 reduction site to the open end at the cytosolic side.

stacking interaction with the adenyl group (Fig. 9B). For the matrix cholate site, the bound (or fitted) ADP is salt-bridged at the two phosphate groups with Arg^{14} and Arg^{17} of subunit VIa. The two sugar hydroxyls and the amino group of ADP are hydrogen-bonded to the phosphate group of PE5 and the main chain carbonyl of Phe^{21} of subunit VIa. Furthermore, the indole of Trp^{275} of helix VII in subunit I belonging to the other monomer also is stacked with the adenyl group. This stacking interaction would contribute to the stability of the dimer under physiological conditions. Thus, the cholate binding sites could be the binding sites for nucleotides proposed to control the enzyme function (*23*). The cholate molecules in the crystal structure are likely to be contaminated during the solubilization of this protein from mitochondrial membrane by the detergent.

Structures participating in proton transfer. Cytochrome c oxidase reduces O_2 to H_2O coupled with the proton pumping, making channels for protons, H_2O, and O_2 a prerequisite to this function. Mutagenesis results suggest two types of proton channels, one for protons for H_2O formation and the other for proton pumping (*24*). Protons are transferred most effectively through hydrogen bonds, particularly in a hydrophobic environment such as the transmembrane region of this enzyme. Thus, we searched for any structure that could participate in a hydrogen-bond network. Neither the network spanning across the transmembrane region from the matrix side to the cytosolic side nor the one from the matrix side to the oxygen reduction site was detectable in our crystal structure. Nevertheless, many cavities (spaces with no detectable electron density distribution) inside the molecule connect short hydrogen-bond systems or pairs of functional groups that could participate in a hydrogen-bonded relay system. These cavities are likely to contain water molecules and thus to conduct protons readily. Furthermore, there are many points where there is space for a conformational change of side chain that would induce a new hydrogen-bond system (possible hydrogen-bond structure). Thus, any conformation change induced by changes in redox or ligand binding states could control proton transfer. In addition, conformation changes could mediate redox or ligand-induced changes in p*K* of ionizable amino acids. Thus a conformationally controlled network composed of hydrogen bonds could function as a proton pump coupled with dioxygen reduction. The following three networks in subunit I are candidates for the proton channels in the enzyme (Fig. 10).

The main part of a network involves residues in helices III and IV of subunit I (Fig. 10A). At the entrance of this network are His^{503} and Asn^{11}, both in extended loops and hydrogen-bonded to a fixed water. The channel terminates at Ser^{142} connected to Ser^{115} with a possible hydrogen-bond structure. The Ser^{115} could form a new hydrogen bond with Ser^{142} when proton release to the cytosolic side is required, and thus serve as a system for preventing undesirable back flow of protons. This channel contains four other possible hydrogen-bond structures between Tyr^{19}, a fixed water hydrogen-bonded to Asn^{98}, Ser^{101} and Ser^{156}. If a conformational change around the almost completely conserved residue, Tyr^{19}, is induced by redox or ligand binding reactions coupled with a p*K* change of at least one of the amino acids in the network, it could provide unidirectional proton transfer. For example, if on dioxygen reduction Tyr^{19} forms a new hydrogen bond with a fixed water connecting Asn^{98}, and concomitantly there is a decrease in p*K* of Asp^{91} which is linked to Asn^{98} via a fixed water with two hydrogen bonds, then proton transfer toward the cytosolic side could be coupled with the dioxygen reduction. All the amino acids in the network are well conserved, although in some species Ser or Thr are replaced with alanine or glycine. Because of the small size of these residues, they could form cavities to contain water and still allow proton transfer.

The second network is located mainly between helices XI and XII of subunit I (Fig. 10B) and contains Asp^{407} at the entrance of the network on the matrix side and only one possible hydrogen bond structure between Asn^{451} and Tyr^{443}. The three residues on the exit—Arg^{38}, Asn^{451} and Tyr^{443}—are highly conserved, suggesting a role in proton transfer in a manner analogous to that of the first network. A branch leading to heme a could control the proton transfer along the main stream by redox changes in heme a.

The third network involving helices VI and VIII of subunit I and heme a_3, (Fig. 10C) spans from Lys^{265} at the entrance to Tyr^{244} connected to His^{240}, a ligand to Cu_B, by a possible hydrogen-bond structure. The other possible hydrogen-bond structure is between Lys^{319} and Thr^{316}. Since this network ends at the ligand to Cu_B, it is most likely to work as a channel for protons to form water molecules. However, it cannot be excluded that this system serves also as a proton pump via the His^{240}, Cu_B, and possibly His^{291}, which is the end of a hydrogen-bond system leading to a water channel as described below. In this case, Cu_B may control p*K* values of the two imidazole ligands to induce a unidirectional proton transfer coupled with the redox state. This mechanism differs from that of Iwata *et al.* (*7*) in that it does not include the dissociation of histidine-Cu_B ligation.

The above three networks form an equilateral triangle when viewed from the cytosolic side such that the proton channel leading to the dioxygen reduction site is equidistant from the two possible proton pumping channels. Proton pumping must be coupled to the redox reaction or ligand binding but could occur remote from the oxygen reduction site per se. Furthermore, more than two pathways could be effective. Thus, we should not exclude any of the above candidates for channel for proton pumping at present. The size and shape of the cavities in Fig. 10 are not drawn quantitatively. Some of the cavities are not large enough for differentiating them clearly from the spaces in possible hydrogen bond structures at the present resolution. Such a small cavity or a possible hydrogen bond structure could block the hydrogen bond network in which the structures are involved, if they do not form any hydrogen bond in any oxidation or ligand binding state. Thus, crystal structures at other oxidation and ligation states are indispensable for identifying the true physiological channels.

A proton pumping pathway to the dioxygen reduction site by way of Ser^{157}, Glu^{242}, and His^{290} from an entrance on the matrix side including Asp^{91} has been proposed for the *Paracoccus* enzyme (*7*). The bottom part of the first network as given above (Fig. 10A) seems essentially the same as that proposed, up to Ser^{157}. Our crystal structure contains a cavity connecting Ser^{157} with Glu^{242}, as in the case of the bacterial enzyme. However, His^{290} is located far from Glu^{242}, giving no evidence of a possible proton transfer in our crystal structure.

Possible channels. A structure that could serve as a water channel for removing H_2O produced at the O_2 reduction site (Fig. 10D), proceeds from the cytosolic side of heme a_3 along the subunit I–II interface to the cytosolic surface of the enzyme. The magnesium site and the propionates of heme a_3 form a hydrophilic environment that includes the two basic amino acids (Arg^{438} and His^{368} of subunit I), the two propionates of heme a_3, Asp^{364} of subunit I, and two fixed waters; all are connected with hydrogen bonds. The hydrophilic region is connected to a channel formed on the interface between subunits I and II with a loose arrangement of hydrophilic residues that could provide a water channel to the cytosolic surface with small conformational changes. All amino acids suggested to be involved in the channel are well conserved in most species so far reported, implying a common mechanism for removing water from the active site. The possible channel in the crystal structure does not have enough space for water molecule to pass through freely, which seems indispensable for preventing proton leak from the cytosolic side.

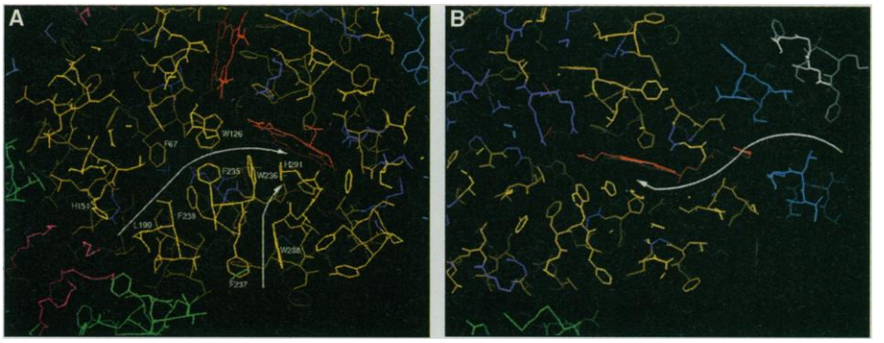

Fig. 11. Possible O_2 channels. Possible channels reaching Cu_B (**A**) and by way of hydroxyfarnesylethyl group (**B**). Red structures are hemes. Blue, green, and white amino acid residues belong to subunit II, III, and VIc, respectively. Yellow amino acid residues are aromatic or hydrophobic in subunit I. A pink structure in (A) is the phospholipid in the lipid pool of subunit III. The white arrows indicate the possible pathways of O_2.

No space through which a dioxygen molecule (O_2, a rod-shaped molecule with the diameter of 2.4 Å) can reach the oxygen reduction site (the Fe_{a3}-Cu_B site) from the molecular surface is detectable, as in the case of hemoglobin and myoglobin (*25*). In analogy to these globins, the conformation with an open channel for O_2 seems attained only during one of the many reversible and rapid conformational changes that occur in protein structure giving populations too low to detect by x-ray crystallography (*26*). However, the O_2 channel (or channels) is probably located in the following three areas near the O_2 reduction site, where most of the amino acid side chains in the area are hydrophobic and packed loosely.

Cu_B occurs near the molecular surface facing the space between monomers where no other subunit is placed. On the surface nearest to Cu_B, is Phe^{237} (Fig. 11A). Next to this Phe, we find Trp^{288}, Trp^{236} and His^{291} located on a line to Cu_B. These side chains, as well as other side chains nearby, provide a hydrophobic environment from the molecular surface to the Cu_B site indicated by the aromatic and hydrophobic residues (Fig. 11A). These residues, which are well conserved, indicate the importance of the hydrophobicity.

Dioxygen molecules could approach the dioxygen reduction site. Starting from His^{151} on the surface of subunit I exposed to the lipid pool of subunit III, a network of hydrophobic amino acids are well conserved including Leu^{199}, Phe^{67}, Phe^{238}, Phe^{235}, Trp^{126}, and Trp^{236} approaches to the dioxygen reduction sites.

The third candidate for the dioxygen channel includes the hydroxylfarnesylethyl group of heme a_3, with the terminal being on the surface of subunit I between the two attaching point of the two transmembrane helices of subunit II (Fig. 11B). The environment of the alkyl group is hydrophobic with loosely packed amino acid side chains so that the dioxygen could pass through to the oxygen binding site with a little change in the conformation around the alkyl group. All the above three channels may be effective under physiological conditions in order for attaining the extremely high affinity of the enzyme to O_2.

Any of the above channels proposed requires some conformational change coupled to the redox reaction at the metal sites in order to function as the proposed channel. Various mechanisms for these processes are possible, depending on the nature of the conformational change. Thus, the discussion on the reaction mechanism should be reserved until the crystal structures at other oxidation states are available.

REFERENCES AND NOTES

1. B. G. Malmström, *Chem. Rev.* **90**, 1247 (1990); G. T. Babcock and M. Wikström, *Nature* **356**, 301 (1992).
2. We follow the terminology of Kadenbach for the subunits of cytochrome c oxidase [B. Kadenbach and P. Merle, *FEBS Lett.* **135**, 1 (1981); B. Kadenbach, U. Ungibaver, J. Jaraush, U. Buge, L. Kuhn-Neutwig, *Trends Biochem. Sci.* **8**, 398 (1983)].
3. R. A. Capaldi, *Annu. Rev. Biochem.* **59**, 569 (1990).
4. O. Warburg and E. Negelein, *Biochem. Z.* **214**, 64 (1929).
5. R. M. Garavito and D. Picot, *Methods* **1**, 57 (1990).
6. T. Tsukihara *et al.*, *Science* **269**, 1069 (1995).
7. S. Iwata, C. Ostermeier, B. Ludwig, H. Michel, *Nature* **376**, 660 (1995).
8. M. Muller, N. Labonia, A. Azzi, *Biochem. Biophys. Res. Commun.* **154**, 1260 (1988); M. Raitio, T. Jalli, M. Saraste, *EMBO J.* **6**, 2825 (1987).
9. A. C. Bloomev, J. N. Champress, G. Bricoqne, R. Staden, A. Klug, *Nature* **276**, 362 (1978).
10. C. Chothia, M. Levitt, D. Richardson, *Proc. Natl. Acad. Sci. U.S.A.* **74**, 4130 (1977).
11. W. H. Andy-Mark *et al.*, *Nature* **367**, 750 (1994).
12. T. Härd *et al.*, *Science* **249**, 157 (1990).
13. Y.-Z. Zhang, G. Ewart, R. A. Capaldi, *Biochemistry* **30**, 3674 (1991).
14. D. N. Beratan, J. N. Onuchic, J. R. Winkler, H. B. Gray, *Science* **258**, 1740 (1992).
15. B. C. Hill, *J. Biol. Chem.* **269**, 2419 (1994).
16. G. A. Palmer, Ed., *Long Range Electron Transfer in Biology* (Dekker, New York, 1991).
17. M. K. F. Wikström, H. J. Harman, W. J. Ingledew, B. Chance, *FEBS Lett.* **65**, 259 (1976).
18. S. Yoshikawa and W. S. Caughey, *J. Biol. Chem.* **257**, 412 (1982).
19. J. E. Morgan, M. I. Verkhovsky, M. Wikström, *J. Bioenerg. Biomembr.* **26**, 599 (1994).
20. B. C. Wang, *Methods Enzymol.* **115**, 90 (1985).
21. N. C. Robinson, *Biochemistry* **21**, 184 (1982).
22. A. O. Vassilev, N. Plesofsky-Vig, R. Brambel, *Proc. Natl. Acad. Sci. U.S.A.* **92**, 8680 (1995).
23. G. Anthony, A. Reiman, B. Kadenbach, *ibid.* **90**, 1652 (1993).
24. J. W. Thomas, A. Puustinen, J. O. Alben, R. B. Gennis, M. Wikström, *Biochemistry* **32**, 10923 (1993); J. A. Garcia-Horsman, A. Puustinen, R. B. Gennis, M. Wikström, *ibid.* **34**, 4428 (1995); J. Fetter *et al.*, *Proc. Natl. Acad. Sci. U.S.A.* **92**, 1604 (1995). These mutagenesis experiments suggest that Asp^{91} and Asn^{98} are indispensable for proton pumping. The two oxygen atoms of Asp^{91} side chain are hydrogen-bonded to main chain imides of His^{12} and Met^{92} (not shown) in addition to the hydrogen bonds to the two fixed waters as stated above. One of the two terminal atoms of Asn^{98} is also hydrogen-bonded to Asn^{80}, in addition to the hydrogen bond to the fixed water, which is also bound to Asp^{91} via a hydrogen bond. Replacement of Asp^{91} to Asn would destroy such a tightly connected structure around Asp^{91} is expected from the mutagenesis results.
25. M. F. Perutz, *Mechanism of Cooperativity and Allosteric Regulation in Proteins* (Cambridge Univ. Press, Cambridge, 1990).
26. W. S. Caughey, H. Shimada, M. G. Choc, M. P. Tucker, *Proc. Natl. Acad. Sci. U.S.A.* **78**, 2903 (1981); W. T. Potter, J. H. Hazzard, M. G. Choc, M. P. Tucker, W. S. Caughey, *Biochemistry* **29**, 6283 (1990).
27. A. Brünger, J. Kuriyan, M. Karplus, *Science* **235**, 458 (1987).

28. Supported in part by Grants-in-Aid for Scientific Research on Priority Area from the Ministry of Education and Culture of Japan [Bioinorganic Chemistry and Cell Energetics (S.Y.), and grants 06276102 and 05244102 (T.T.), Grant-in-Aid (06558102 to T.T.)] and from the New Energy and Industrial Technology Development Organization of Japan [Grant-in-Aid for the Proposal-Based Advanced Industrial Technology R&D Program (B-021 to S.Y.)]. The project was done with the approval of the Photon Factory Advisory Committee, and the National Laboratory for High Energy Physics, Japan (Proposal number 91-050 and 94G-041). We thank N. Sakabe, A. Nakagawa, N. Watanabe, and S. Ikemizu for assisting in data collection with the Weissenberg camera and synchrotron radiation.

22 November 1995; accepted 20 March 1996